Available online at www.sciencedirect.com
ScienceDirect
Journal of Magnetic Resonance 192 (2008) 85–91
JMR Journal of Magnetic Resonance
www.elsevier.com/locate/jmr

Theoretical prediction and experimental measurement of the field dependence of the apparent transverse relaxation of hyperpolarized noble gases in lungs

Juan Parra-Robles [a], William Dominguez Viqueira [a], Xiaojun Xu [a], Alexei Ouriadov [a], Giles E. Santyr [a,b,c,*]

[a] Imaging Research Laboratories, Robarts Research Institute, P.O. Box 5015, 100 Perth Drive, London, Ont., Canada N6A 5K8
[b] Department of Medical Biophysics, The University of Western Ontario, London, Ont., Canada N6A 5C1
[c] Department of Diagnostic Radiology and Nuclear Medicine, The University of Western Ontario, London, Ont., Canada N6A 5A5

Received 8 July 2007; revised 1 February 2008
Available online 14 February 2008

Abstract

In this work, computer modeling based on a finite element method is used to simulate the T_2^* relaxation of hyperpolarized noble gases (HNG) in the lungs. A physical model of lung airways consisting of a phantom constructed from micro-capillary fibers of diameters similar to the size of lung airways with semi-permeable walls is also presented. The fibers are surrounded by a liquid medium (water) of magnetic susceptibility similar to lung tissue. Theoretical predictions of the field strength dependence of T_2^* for ^{129}Xe in the phantom and in vivo rat lung are presented. These predictions are in good agreement with experimental T_2^* values obtained from the phantoms and in vivo rat lungs (160, 19 and 8 ms) at three different field strengths (0.074, 1.89 and 3 T, respectively) using hyperpolarized ^{129}Xe. The strong dependence of T_2^* on field strength is consistent with the theoretical prediction that low fields may be optimal for HNG MR imaging of the lungs as the decreased T_2^* at high fields necessitates an increase in bandwidth for conventional MR imaging.

Keywords: T_2^*; Field dependence; Lung; Hyperpolarized noble gas; Computer modeling

1. Introduction

Hyperpolarized noble gas (HNG), ^{3}He (helium) or ^{129}Xe (xenon), MR imaging has become a promising approach for visualizing lung anatomy and function. HNG MR parameters, such as the apparent transverse relaxation time (T_2^*), magnetic susceptibility difference ($\Delta\chi$) and apparent diffusion coefficient (ADC) are sensitive to the geometric and physiological properties of the airways and may provide a means of diagnosing lung diseases such as chronic obstructive pulmonary disease (COPD) and emphysema [1,2].

Several theoretical models have been proposed to understand the relationship between these MR parameters and lung anatomical and physiological parameters (e.g. average airway/alveolar size, membrane thickness and gas permeability) and to optimize their measurement (e.g. pulse sequence, ventilation conditions, gas mixture). In particular, the signal-to-noise ratio (SNR) and spatial resolution of HNG MR imaging is predicted to depend on ADC and T_2^* [3], the latter expected to depend strongly on field strength and an important factor in determining the optimum configuration of an MR system for HNG imaging of the lungs [3].

Wild et al. [4] investigated the effects of macroscopic background field gradients upon 2D gradient echo images of inhaled ^{3}He in the human lung at 1.5 T and demonstrated effective compensation of in-slice signal loss in ^{3}He gradient echo images using a multiple acquisition

* Corresponding author. Address: Imaging Research Laboratories, Robarts Research Institute, P.O. Box 5015, 100 Perth Drive, London, Ont., Canada N6A 5K8. Fax: +1 519 663 3900.
E-mail address: gsantyr@imaging.robarts.ca (G.E. Santyr).

1090-7807/$ - see front matter © 2008 Elsevier Inc. All rights reserved.
doi:10.1016/j.jmr.2008.02.009

interleaved single gradient echo sequence. Salerno et al. [5] measured the T_2^* of ^{3}He gas in the lung and compared the effects of susceptibility-induced magnetic field inhomogeneities on the appearance of lung images at 1.5 T and 0.54 T. They reported mean T_2^* values for ^{3}He gas in the healthy human lung of 26.8 ± 1.5 ms and 67.9 ± 1.3 ms at 1.5 and 0.54 T, respectively. At 0.54 T, interleaved-spiral images showed markedly less blurring due to susceptibility effects compared to images acquired at 1.5 T.

Chen et al. [6] have studied the helium spectrum lineshape in live guinea pig lungs. The frequency shifts of the peaks observed in the helium spectra were analyzed using a simple model of isolated cylindrical and spherical compartments in the presence of a uniform magnetic field, for the estimation of susceptibility-induced field gradients. They also demonstrated spatially resolved measurements of T_2^* in humans and guinea pigs using helium and xenon [7] at 1.5 T. The behavior of T_2^* in the different diffusion regimes (e.g. free, restricted and localized diffusion) was predicted by treating the lung as a porous medium with spherical isolated pores. However, the use of such simple geometries has been demonstrated to significantly underestimate susceptibility-induced field gradients (i.e. field inhomogeneity) expected near the very irregular boundaries between tissue and gas space present in actual lung tissue [8]. Furthermore, simple models do not account for the effects of neighboring airways, anisotropy and branching on the susceptibility-induced gradients expected to influence T_2^*.

More realistic models have been presented to describe HNG diffusion in the lungs. Yablonskiy and coworkers [9] introduced an analytical model that considers the airways as a large number of infinitely long cylinders, randomly oriented in all directions. This model accounts for the anisotropy of diffusion in the lungs and allows the estimation of the average radii of the alveolar ducts and two orientation-dependent diffusion coefficients (longitudinal and transverse ADC), however the model fails to demonstrate the substantial differences in ADC measured between normal and emphysematous lungs at the acinar level. Fichele et al. [10,11] have used finite difference methods to numerically simulate more realistic alveolar ducts. Their results were in reasonable agreement with Yablonskiy's model, but found that the average airway radii were consistently overestimated. They also simulated diffusion in more complex structures in 2D (e.g. porous media and tree-like and grape-like geometries) [11] which accounts for a range of sizes of airways, but this work focused only on ADC and evaluation was done by comparison to histological parameters not immediately related to lung airway sizes (e.g. mean linear intercept) [12,13]. Furthermore, direct comparison to histology is not always possible and has limitations (e.g. reproducibility of lung inflation state [14], tissue preservation). Experimental validation of HNG diffusion models in realistic test objects (i.e. phantoms) of controlled (known) geometry and dimensions similar to lung airways has not yet been reported. Furthermore, Fichele's model has not yet been extended to numerically simulate the effects of the background gradients (field inhomogeneities) induced by the susceptibility differences at the gas–tissue interface. Diffusion in these background gradients is one of the main mechanisms of T_2^* relaxation of HNG in the lungs.

In this work, we use computer modeling to extend Fichele's model to include susceptibility effects for T_2^* simulation and compare the results with measurements obtained from a physical model and in vivo in rat lungs. Computer modeling was based on a finite element method to allow incorporation of susceptibility-induced background field inhomogeneities. The physical model consisted of a phantom constructed from micro-capillary fibers of diameters similar to the size of lung airways with semi-permeable walls, which are surrounded by a liquid medium (e.g. water) of magnetic susceptibility similar to lung tissue. Theoretical predictions of the field strength dependence of T_2^* for ^{129}Xe in the phantom and in vivo rat lung are presented. These predictions are compared with experimental T_2^* values obtained from the phantom and in vivo rat lung at three different field strengths (0.074, 1.89 and 3 T) using hyperpolarized ^{129}Xe. The implications of the strong field dependence of T_2^* on HNG MR imaging and the potential for using capillary phantoms to study other lung properties such as diffusional anisotropy [9] and gas exchange are discussed.

2. Methods

2.1. Computer modeling

The behavior of the complex transverse magnetization M ($M = M_x + i\ M_y$ where i is the imaginary unit) in the rotating frame of reference, in the presence of magnetic field inhomogeneity $\Delta\vec{B}_0$ and gradient $\vec{G}$ is described by Fichele et al. [11]:

$$\frac{\mathrm{d}M(\vec{r},t)}{\mathrm{d}t} = -\mathrm{i}\gamma[\Delta B_0(\vec{r}) + \vec{G}(\vec{r},t)\cdot\vec{r}]M(\vec{r},t) + D\nabla^2 M(\vec{r},t) \tag{1}$$

where D is the free diffusion coefficient of the gas, γ is the gyromagnetic ratio and $\vec{r}$ is the spatial position vector. ΔB_0 includes the static field inhomogeneities (system-related) and the inhomogeneities induced by magnetic susceptibility differences ($\propto \Delta\chi(\vec{r})B_0$) in the sample.

Eq. (1) was solved numerically using a finite element method for the geometries of interest in this work to obtain values of T_2^* (without an applied gradient). Models of an alveolar duct and capillary tubes, used to simulate the rat lung and the phantom, respectively, are shown in Fig. 1. The static field inhomogeneities induced by susceptibility differences at the tissue–gas interface and the behavior of the magnetization in the transverse plane in the presence of diffusion (by solving Eq. (1))

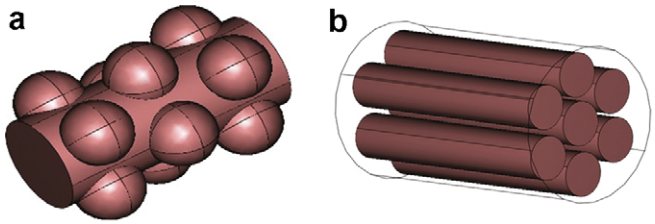

Fig. 1. Computer models of an alveolar duct (left) and capillary phantom (right) used in the simulations. For the T_2^* simulations, they were considered to be surrounded by water.

were simulated using Comsol Multiphysics (COMSOL AB, Stockholm, Sweden).

For the T_2^* simulations, the magnetostatic problem (with continuity at the gas–water interfaces) was solved initially to obtain the magnetic field strength deviations (ΔB_0) due to the susceptibility differences at the gas–tissue interface. The presence of capillary walls in the phantom was not included in the modeling since their magnetic susceptibilities (e.g. −7.04 ppm to −9.93 ppm for polypropylene fibers depending on thickness, elongation and orientation with respect to the field [15]) are similar to the magnetic susceptibility of water (−9.05 ppm). The magnetic susceptibility of the gas in the alveolar duct simulations was assumed to be 0.11 ppm, due to the presence of paramagnetic molecular oxygen (see Ref. [7] for calculation details). To simulate the phantom experiments, where the oxygen is removed before delivering the gas (see details below), the magnetic susceptibility ($\sim 10^{-10}$) was assumed to be 0 ppm.

The calculated field distributions were then incorporated into the diffusion simulation. The behavior of the MR signal at every point in the object was obtained as the time-dependent solution of Eq. (1) and the bulk signal was then obtained as the volume integral of the solution for each time step and used to estimate the bulk T_2^* (i.e. the time constant of the transverse magnetization decay).

For diffusion calculations, the boundary conditions were similar to those used by Fichele et al. [10,11], while the dimensions of the alveolar duct model (Fig. 1) were scaled down to match the dimensions of rat airways (i.e. alveolar radius: 0.04 mm, overall duct radius: 0.08 mm and spacing between groups of alveoli: 0.1 mm). Boundary conditions assumed impenetrable walls (zero flow through the walls) on all surfaces except the ends of the cylinders and ducts, where periodic boundary conditions with phase-wrapping [10,11] were assumed. To simulate the different orientations of lung airways with respect to the magnetic field direction (B_0), the calculated bulk signal was considered to be a summation of the signals calculated for one alveolar duct, at 30 different field orientations (ranging from 0 to π) [10].

All the geometric models were built using Comsol Multiphysics and then exported to Comsol Script, where the solutions for each time step and field orientation were obtained and the results processed (i.e. volume integration, T_2^* estimation).

2.2. Physical model of alveolar duct

A physical model of the alveolar duct (i.e. phantom) was constructed based on micro-capillary tubing used in dialysis and microfiltration modules (Spectrumlabs, Rancho Dominguez, CA, USA) (Fig. 2). These capillaries have dimensions similar to the respiratory airways (0.2 mm inner diameter). Although the distribution of variations of the actual capillary diameters about the mean diameter was not known, it was expected to contribute negligibly to the model and was not considered in our calculations. The capillaries were arranged in a co-linear bundle (Figs. 1 and 2) and were surrounded by a liquid medium (e.g. water). The capillary walls (thickness 0.04 mm) are made from a semi-permeable membrane (polypropylene).

2.3. HNG production and delivery to phantoms

Hyperpolarized natural abundance xenon gas (26.4% ^{129}Xe) was produced using a continuous-flow polarization system that used a 60 W diode array laser ($\lambda = 794.8$ nm, Coherent, Santa Clara, USA) and a gas mixture of 1% xenon, 10% nitrogen and 89% helium and produced ^{129}Xe polarizations of up to 22% [16,17]. In order to minimize depolarization of the hyperpolarized ^{129}Xe by paramagnetic molecular oxygen, the air inside the phantom was initially flushed out by flowing the gas mixture through the phantom for about 30 s. The phantom was then evacuated using a syringe and a three-way valve, before delivering pure hyperpolarized xenon (cryo-trapped using liquid

Fig. 2. Phantom used to simulate airways properties in the T_2^* measurements.

nitrogen) gas using a different syringe. A one-way valve fitted at the phantom outlet prevented air from re-entering the phantom during the evacuation process, while keeping the pressure inside the phantom at 1 atm.

The polarizer was located in close proximity to the MR imaging system, allowing the flowing gas to be delivered directly to the bore of the magnet for shimming (1% xenon gas mixture). For the experiments involving pure hyperpolarized xenon gas, the xenon ice was first collected in the field of a 0.3 T permanent magnet and then transferred to the bore of the MR imaging system where the ice was rapidly thawed before being delivered to the phantom or custom animal ventilator (described below).

2.4. Animal preparation and ventilation

This study was approved by the University of Western Ontario Council on Animal Care using a protocol described elsewhere [18]. Two male Brown Norway rats (Charles River Laboratories, Saint-Constant, Canada) were used at each field strength. The rats were initially anesthetized with 3.0% Isoflurane (Abbott Laboratories, Saint-Laurent, Canada) through a nosecone using a vaporizer (VetEquip, Pleasanton, CA). Rats remained anesthetized by intravenous administration of a 10:1 mixture of Propofol (Astra Zeneca, Mississauga, Canada), and Ketamine (Bioniche Animal Health, Belleville, Canada) at a rate of approximately 45–60 mg/kg/h. Rats were intubated with a 5-French polypropylene urinary catheter (Sherwood Medical, St. Louis, MO) held in place with three sutures tied around the trachea to ensure an airtight seal, and ventilated in the supine position with a custom ventilator (GE Healthcare, Malmo, Sweden) compatible with MR imaging of hyperpolarized noble gases. To ensure the health of the animal, blood oxygenation and heart rate were monitored using an optical transducer (LifeSense Vet, MedAir, Delsbo, Sweden) on the hind paw ($SpO2 > 90\%$).

For MR experiments, animals were ventilated with the following settings: respiratory rate of 80 breaths/min, peak inspiratory pressure of 12 cm H_2O, tidal volume of 8 mL per kg of animal body mass and inspiratory/expiratory times of 0.5 s each. Inspiratory pressure was monitored during experiments at a rate of 10 samples/s using a pressure transducer (HCXM050D6V, Sensor Technics, Puchheim, Germany) connected to a pneumatic valve assembly attached to the endotracheal catheter. The valve assembly allowed computer-controlled switching between air and the HNG in the pressured reservoir with minimal depolarization. Equal inspiratory pressures, and as a result, application of equal volumes of pure HNG or air as required during one breath cycle of each gas was ensured by regulating the gas flow from the reservoir with a needle valve (Air Logic, Racine, WI) in conjunction with appropriate flow restricting orifices (Air Logic, Racine, WI). Tidal volumes for each gas were calibrated by water displacement. The inspiratory pressure transducer was calibrated separately during 11 s breath holds using a water manometer (Uniweld, Fort Lauderdale, FL). For each breath-hold during in vivo experiments, the pressure was observed to peak at ~1 s and then established a steady-state after 2 s following the end-inspiration at which point the MR experiment was triggered.

The hyperpolarized ^{129}Xe was expanded from xenon ice directly into a 260 mL plastic bag (Tedlar, Jensen Inert, Coral Springs, FL) for MR experiments. Prior to transfer of hyperpolarized ^{129}Xe, the bag was rinsed 3 times with nitrogen gas, and subsequently vacuumed (100 mtorr) to minimize depolarization of gas caused by oxygen. The bag was then placed in the pressurized reservoir attached to the ventilator [18].

2.5. MR experiments

MR experiments were conducted at three magnetic field strengths: 0.074, 1.89 and 3 T. Experiments at 1.89 T were performed using an animal MR system (Magnex, Yarnton, Oxon, England) and 3.0 T experiments used a whole body MR system (Signa EXCITE, GE Healthcare, Waukesha, WI) using transmit-receive birdcage coils (Morris Instruments, Ottawa, Canada) tuned to the ^{129}Xe resonance frequencies (20 and 35 MHz, respectively).

For the 0.074 T experiments, a broadband, variable field strength (0.01–0.15 T) MR system for rodent imaging was designed and built. The system was based on a water-cooled six-coil electromagnet capable of providing field strengths up to 0.15 T and described in more detail elsewhere [19]. The entire system was controlled by an Apollo imaging console (TECMAG, TX, USA), capable of operating between 0.1 and 100 MHz. Custom-built saddle coils tuned to 0.866 MHz ($B_0 = 0.074$ T) were used [19].

Before the experiments, the field homogeneity at each field strength was optimized by active (i.e. resistive) shimming using signals obtained from a 10 cm diameter spherical xenon phantom. After shimming, the measured linewidths corresponded to inhomogeneities of 8, 2 and 1 ppm at 0.074, 1.89 and 3 T, respectively. This background inhomogeneity was incorporated into the numerical calculations assuming, to a first approximation, that $\Delta\vec{B}_0$ increases linearly with the distance from the center of the region of homogeneity (i.e. geometric center of the sample).

Free induction decay (FID) signals were obtained after a single 90° RF pulse from the phantom and in vivo rat lungs. No filtering was used during the signal acquisition with 2048 samples with readout times of 500, 50 and 25 ms at 0.074, 1.89 and 3 T, respectively. The readout times were selected to be approximately 3 times the expected T_2^* at each field, in order acquire the complete FID while maximizing the SNR (i.e. minimizing the bandwidth). Bulk T_2^* values were estimated by fitting the xenon spectra to a Lorentzian lineshape (i.e. assuming that ^{129}Xe nuclei are in the restricted diffusion regime [7]).

3. Results and discussion

Fig. 3 shows the magnetic field distributions ΔB_0 (deviation from the field in air only) produced by susceptibility differences in the computer models of the alveolar duct and capillary phantom. As expected, field gradients are stronger in the direction of the external magnetic field (horizontal direction) and near the sharpest edges or the alveolar duct. In addition, significant field gradients are introduced by neighboring airways (capillaries) in the phantom model; this can be appreciated by comparing the field distribution in the central capillary to the distributions in the rest of the capillaries. Simulations show that these regions of large susceptibility-induced gradients contribute significantly to the observed T_2^*, which decreases with increased field strength as shown in Fig. 4.

The experimentally measured ^{129}Xe T_2^* values in the phantom are in good agreement with the results of the computer simulations (Table 1) and with the T_2^* values measured in vivo in rat lungs. On closer inspection, measured T_2^* values in the phantom at 0.074 T were lower (statistically significant, $p = 0.013$) than the calculated values, presumably because the length of the phantom was larger than the region of homogeneity of the magnet, resulting in a field inhomogeneity larger than the value used in the simulations (8 ppm).

Both calculated and measured T_2^* values at low magnetic fields were considerably larger than at high field. At low field strength, the T_2^* is dominated by the background field inhomogeneity. No line broadening due to lung susceptibility effects (with respect to a gas-filled syringe of similar volume) was observed. At high field, the non-linear dependence of T_2^* on the field strength (Fig. 4) suggest that T_2^* is dominated by susceptibility-induced microscopic field gradients (averaged out by diffusion). Although a detailed study of the relative contributions of these two relaxation mechanisms was outside the scope of this work, the distinction is very important and may be investigated in the future using the models and methods presented here.

The strong dependence of T_2^* on field strength is consistent with the theoretical prediction [3] that low fields may be optimal for HNG MR imaging of the lungs as the decreased T_2^* at high fields necessitates a concomitant increase in bandwidth for conventional MR imaging thereby reducing SNR. In addition to SNR and spatial resolution considerations, the long T_2^* values available at low fields would allow investigation of different scales of airway sizes using long range diffusion measurements with diffusion times up to significantly larger values (e.g. 1–150 ms) without the use of stimulated echoes (i.e. encoding diffusion in the transverse direction rather than the longitudinal direction [20]).

The computer model of lung airways presented in this work is currently limited to single airways with impenetrable walls at the acinar level. The model could be modified

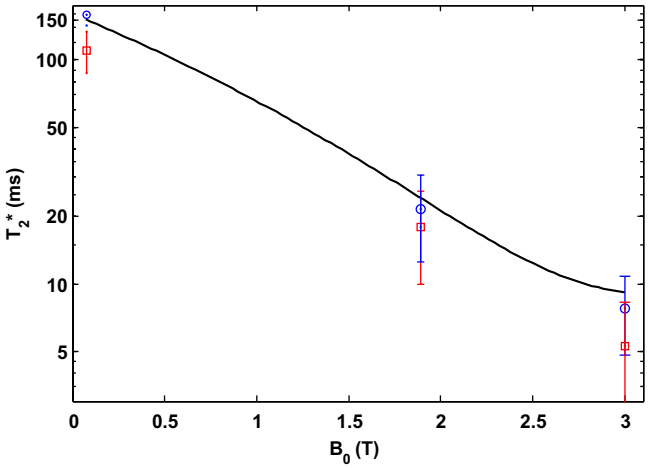

Fig. 4. Field dependence of xenon T_2^* obtained from simulations (solid line) and phantom (squares) and rat lung (circles) measurements.

Table 1
Comparison of the calculated (simulation) and measured T_2^* values

	Simulation (phantoms) (ms)	Simulation (rats) (ms)	Phantom (ms)	Rat lungs (ms)
0.07 T	150	150	109 ± 9	160 ± 11
1.89 T	25	28	20 ± 5	19 ± 6
3 T	8.3	9.5	6 ± 2	8 ± 3

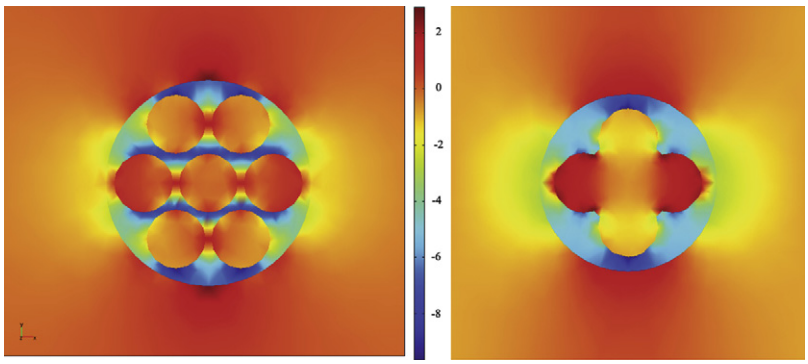

Fig. 3. Computer simulation of the magnetic field strength variation (ΔB_0, transverse plane, in ppm with respect to the field in air) induced by susceptibility differences in the capillary phantom (left) and alveolar duct (right) models. The magnetic field (1.89 T) is oriented along the horizontal direction. The airspaces are assumed to be surrounded by water-like media (tissue).

to simulate the complex 3D lung geometry (e.g. airway branching, varying airway sizes) and the effects of xenon exchange between the gas space and tissue (not relevant for helium, which is practically insoluble in tissue). These modifications may provide additional insight into the relationship between T_2^* measurements and anatomical and physiological changes produced in the lungs by disease. The development of such a complex model was not attempted in this work due to the associated computational requirements. This would be a very worthwhile goal of future work.

Although the reasonable agreement between measurements and calculation seems to suggest that our model can predict T_2^* values in the lungs, the susceptibility effects of neighboring airways (modulated by the field averaging effect of diffusion) in the complex geometry of the lung deserve further attention in the future. Macroscopic susceptibility effects, in particular those induced by the presence of other organs and body tissues also need to be included in a more complete model since experimental measurements [7] have shown that local T_2^* values obtained from imaging sequences (i.e. T_2^* maps) can significantly deviate from bulk T_2^* values obtained from the whole lung as described here.

Although the phantom has semi-permeable walls, no significant effects of xenon exchange with the water compartment were observed. This was verified by inspecting the xenon spectra. No dissolved ^{129}Xe peaks ($\sim$200 ppm) were observed along with the gas peaks. We have shown that higher gas pressures and/or larger capillary surface area and pore sizes are necessary to observe a dissolved peak (data not shown). Similarly, water was not be able enter the fibers through the pores if operated within the range of pressures differences specified by the manufacturer. This was confirmed visually by verifying the absence of any water in the gas outlet of the dialysis module.

However, the phantom does present airway dimensions and geometry similar to lung airways, and offers characteristics that can potentially be exploited to simulate other properties of HNG in lung airways which may be explored in future. Among these characteristics are: (i) a range of packing and sizes of capillaries are available to simulate the airway distribution in the lungs, (ii) the orientation of the fibers can be changed (e.g. wrapping the fibers in a spiral pattern) to simulate and distribution of airway orientations anisotropy [9] and (iii) fibers with larger wall permeability (pore sizes) and surface area can be used to simulate different conditions of gas exchange in the lungs and the measurement of xenon diffusing capacity [21].

4. Conclusions

This work has demonstrated that computer simulations using finite elements is a useful tool to predict the T_2^* values of HNG in the lungs with reasonable accuracy by incorporating realistic geometries, diffusion effects and calculated susceptibility-induced inhomogeneities. The field dependence of T_2^* obtained from the computer simulation was in good agreement with measurements in physical models of the lung and in rat lungs in vivo. It has also been demonstrated that a physical model of the lungs (i.e. phantom) based on dialysis capillary fibers closely simulates the T_2^* values measured for HNG in the lungs.

References

[1] B.M. Goodson, Nuclear magnetic resonance of laser-polarized noble gases in molecules, material, and organisms, J. Magn. Reson. 155 (2002) 157–216.
[2] M. Salerno, T.A. Altes, J.P. Mugler III, et al., Hyperpolarized noble gas MR imaging of the lung: potential clinical applications, Eur. J. Radiol. 40 (2001) 33–44.
[3] J. Parra-Robles, A.R. Cross, G.E. Santyr, Theoretical signal-to-noise ratio and spatial resolution dependence on the magnetic field strength for hyperpolarized noble gas magnetic resonance imaging of human lungs, Med. Phys. 32 (2005) 221–229.
[4] J.M. Wild, S. Fichele, N. Woodhouse, et al., Assessment and compensation of susceptibility artifacts in gradient echo MRI of hyperpolarized 3He gas, Magn. Reson. Med. 50 (2003) 417–422.
[5] M. Salerno, J.R. Brookeman, E.E. de Lange, J.P. Mugler III, Hyperpolarized 3He lung imaging at 0.5 and 1.5 Tesla: a study of susceptibility-induced effects, Magn. Reson. Med. 53 (2005) 212–216.
[6] X.J. Chen, M.S. Chawla, G.P. Cofer, et al., Hyperpolarized ^{3}He NMR lineshape measurements in the live guinea pig lung, Magn. Reson. Med. 40 (1998) 61–65.
[7] X.J. Chen, H.E. Moller, M.S. Chawla, et al., Spatially resolved measurements of hyperpolarized gas properties in the lung in vivo. Part II: $T2^*$, Magn. Reson. Med. 42 (1999) 729–737.
[8] K.J. Dunn, Enhanced transverse relaxation in porous media due to internal field gradients, J. Magn. Reson. 156 (2002) 171–180.
[9] D.A. Yablonskiy, A.L. Sukstanskii, J.C. Leawoods, et al., Quantitative in vivo assessment of lung microstructure at the alveolar level with hyperpolarized ^{3}He diffusion MRI, Proc. Natl. Acad. Sci. USA 99 (5) (2002) 3111–3116.
[10] S. Fichele, M.N.J. Paley, N. Woodhouse, et al., Finite-difference simulations of ^{3}He diffusion in 3D alveolar ducts: comparison with the "cylinder model", Magn. Reson. Med. 52 (2004) 917–920.
[11] S. Fichele, M.N.J. Paley, N. Woodhouse, et al., Investigating ^{3}He diffusion NMR in the lungs using finite difference simulations and in vivo PGSE experiments, J. Magn. Reson. 167 (2004) 1–11.
[12] G. Peces-Barba, J. Ruiz-Cabello, Y. Cremillieux, et al., Helium-3 MRI diffusion coefficient: correlation to morphometry in a model of mild emphysema, Eur. Respir. J. 22 (2003) 14–19.
[13] J.C. Woods, C.K. Choong, D.A. Yablonskiy, et al., Hyperpolarized ^{3}He diffusion MRI and histology in pulmonary emphysema, Magn. Reson. Med. 56 (2006) 1293–1300.
[14] L. de Rochefort, A. Vignaud, X. Maitre, et al., Influence of lung filling on $T2^*$ values in human at 1.5 T with hyperpolarised ^{3}He, in: Proceedings of the 11th ISMRM meeting, Toronto, Ontario, Canada, 2004, p. 2724.
[15] M. Rakos, R. Simo, Z. Varga, Magnetic study of elongated polypropylene fibers Czechoslovak, J. Phys. 16 (2) (1966) 112–118.
[16] I.L. Moudrakovski, S. Lang, C.I. Ratcliffe, B. Simard, G. Santyr, J. Ripmeester, Chemical shift imaging with continuously flowing hyperpolarized xenon for the characterization of materials, J. Magn. Reson. 144 (2000) 372–377.
[17] J. Parra-Robles, A.R. Cross, G.E. Santyr, Passive shimming of the fringe field of a superconducting magnet for ultra-low field hyperpolarized noble gas MRI, J. Magn. Reson. 174 (2005) 116–124.

[18] G.E. Santyr, W.W. Lam, A. Ouriadov, Rapid and efficient mapping of regional ventilation in the rat lung using hyperpolarized ^{3}He with flip angle variation for offset of RF and relaxation (FAVOR), Magn. Reson. Med., in press.

[19] W. Dominguez Viqueira, J. Parra-Robles, M. Fox, et al., A variable field strength system for hyperpolarized noble gas mr imaging of rodent lungs, Concepts Magn. Reson. B, in press.

[20] C. Wang, G. Wilson Miller, et al., Time dependence of 3He diffusion in the human lung: measurement in the long-time regime using stimulated echoes, Magn. Reson. Med. 56 (2006) 296–309.

[21] N. Abdeen, A.R. Cross, G. Cron, S. White, T. Rand, D. Miller, G.E. Santyr, Measurement of xenon diffusing capacity in the rat lung by hyperpolarized 129Xe MRI and dynamic spectroscopy in a single breath-hold, Magn. Reson. Med. 56 (2006) 255–264.